Journal of Alloys and Compounds 509 (2011) 6980–6986

Contents lists available at ScienceDirect

Journal of Alloys and Compounds

journal homepage: www.elsevier.com/locate/jallcom

Effect of sintering temperature and time on densification, microstructure and properties of the PZT/ZnO nanowhisker piezoelectric composites

Da-Wei Wang[a], Mao-Sheng Cao[a,*], Jie Yuan[b], Ran Lu[a], Hong-Bo Li[a], Hai-Bo Lin[c], Quan-Liang Zhao[a], De-Qing Zhang[a]

[a] School of Materials Science and Engineering, Beijing Institute of Technology, Beijing 100081, China
[b] School of Information Engineering, Central University for Nationalities, Beijing 100081, China
[c] China Astronautics Standards Institute, Beijing 100071, China

ARTICLE INFO

Article history:
Received 7 November 2010
Received in revised form 21 March 2011
Accepted 23 March 2011
Available online 9 April 2011

Keywords:
Composite materials
PZT
Sintering
Piezoelectricity

ABSTRACT

Lead zirconate titanate (PZT) based piezoelectric composites embedded with ZnO nanowhiskers (ZnO_w) were investigated to clarify the optimal sintering condition for densification, microstructure, and electrical properties. The samples are characterized by X-ray diffraction analysis and scanning electron microscopy. The results show that the increase of the sintering temperature and time is quite effective in improving the densification and piezoelectric properties of the PZT/ZnO_w composites. However, the relative density and piezoelectric properties deteriorate as the composites are sintered over the optimal sintering condition. Particularly, the PZT/ZnO_w composites sintered at 1150 °C for 2 h show excellent electrical properties of piezoelectric constant $d_{33} \sim 471$ pC/N, relative dielectric constant $\varepsilon \sim 3838$, planar electromechanical coupling factor $k_p \sim 0.543$, remnant polarization $P_r \sim 23.2$ μC/cm^2 and coercive field $E_c \sim 9.2$ kV/cm.

1. Introduction

The ferroelectric and piezoelectric nature of lead zirconate titanate (PZT) ceramics has led to numerous applications in electronic devices, such as actuators, sensors, capacitors, resonators and high-power transducers [1–5]. The high dielectric and piezoelectric properties of PZT ceramics are obtained for compositions close to the morphotropic phase boundary (MPB), which is located around the $PbZrO_3$:$PbTiO_3$ ratio of 1:1 [6–10]. Furthermore, PZT ceramics could be modified or doped with different additives, which make them more attractive for specific applications [11–18]. Although PZT ceramics have excellent electrical properties, poor mechanical properties such as fracture strength and toughness have been reported. In some applications at high power and high stress, their poor mechanical and electrical reliability become a critical limitation [19–23]. In the past few years, a few studies have dealt with improving the mechanical properties of PZT ceramics by incorporating polymers, particles, oxides, metals, fibers or whiskers [24–38]. However, the electrical properties of PZT-based composites have been deteriorated greatly. Therefore, it is still a challenge to fabricate the PZT-based composites possessing excellent mechanical and electrical properties.

ZnO nanostructures have received considerable attention on potential applications with specific piezoelectric [39], optoelectronic [40–43], electrical [44–47] and microwave absorption properties [48–54] for several decades. Recently, various ZnO nanostructures have been used in polymers, ceramics and films as additives to improve their electrical and mechanical properties [55–63]. Furthermore, the incorporation of ZnO powders in piezoelectrics can result in lower sintering temperature and improved electrical properties [64–68]. Therefore, it is expected that ZnO nanostructures embedding in PZT composites would be a good solution to improve the mechanical behaviors without deteriorating electrical properties severely. Due to their high-temperature strength and excellent chemical stability, ZnO nanowhiskers (ZnO_w) have been used for industrial applications as reinforced composite materials [69–73]. However, there is limited work on the PZT composites embedded with ZnO_w. According to our recent studies [74–77], the incorporation of ZnO_w can improve the mechanical properties of PZT-based composites greatly. Compared with the monolithic PZT, the PZT/ZnO_w composites with 2 wt.% ZnO_w exhibit the optimal mechanical properties and good piezoelectric properties, which are promising candidates for further application [76,77].

For practical production and application, in this work, we have focused on the preparation of PZT/2 wt.% ZnO_w composites at different process conditions (sintering temperature and time) and investigated their sintering, microstructure, piezoelectric and ferroelectric properties in detail. Furthermore, the temperature

* Corresponding author. Tel.: +86 01068914062.
E-mail addresses: caomaosheng@bit.edu.cn (M.-S. Cao), yuanjie4000@sina.com (J. Yuan).

0925-8388/$ – see front matter © 2011 Elsevier B.V. All rights reserved.
doi:10.1016/j.jallcom.2011.03.186

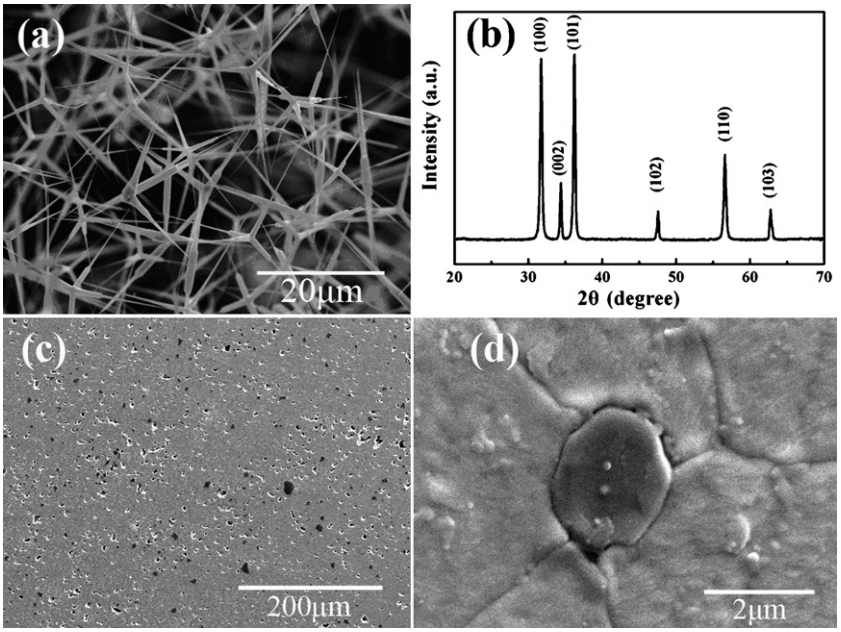

Fig. 1. (a) SEM micrograph of ZnO_w, (b) XRD pattern of ZnO_w, (c) SEM micrograph of polished surface for the PZT/ZnO_w composites sintered at 1150 °C for 2 h and (d) typical morphology of ZnO_w embedded in the PZT matrix.

stability and aging problem of the composites have also been studied.

2. Experimental procedures

The fabrication of PZT/2 wt.% ZnO_w composites was performed by a conventional solid-state sintering. The ZnO_w were synthesized by combustion oxidation of fine zinc powders (purity 99.999%) without any catalysts or additives. Detailed discussion on the synthesis of ZnO_w has been reported elsewhere [78,79]. Commercially available PZT powders (PZT-5MN, Hongsheng Industry, Baoding, China) were used as the raw material. Appropriate amounts of the PZT powders mixed with the as-fabricated ZnO_w for the designated composites (the weight of each condition is about 100 g) were ball milled for 24 h with zirconia balls as the grinding media and alcohol as the solvent. After milling, the slurry was dried at room temperature and then the dried powders were mixed with proper amount of polyvinyl alcohol (PVA) liquid binder addition. The mixed powders were compacted into discs by die pressing. After the binder was burning out in a furnace, the green compacts were sintered from 900 to 1250 °C for 0–4 h in a sealed alumina crucible that contained $PbZrO_3$ powders to minimize lead volatilization. Then all sintered samples were annealed at 900 °C for 5 h in order to alleviate residual stress. Silver paste was printed to form electrodes on both sides of the disc samples, and then fired at 800 °C for 10 min. Poling treatment was carried out in silicon oil at 120 °C for 30 min with an electric field of 3 kV/mm.

The bulk density was determined by the Archimedes method in distilled water. The crystalline phases of the sintered samples and whiskers were examined by the X-ray diffraction (XRD with Ni-filtered Cu Kα radiation). The morphologies of the whiskers and composites were studied by a scanning electron microscopy (SEM, Hitachi S-4100, Japan). The piezoelectric constants d_{33} of the polarized specimens were measured using a ZJ-3AN piezoelectric tester. The relative dielectric constant ε and planar electromechanical coupling factor k_p were calculated with a Model HP 4194 impedance analyzer. In addition, the hysteresis loops and ferroelectric properties were measured using a Radiant Precision Workstation ferroelectric tester system.

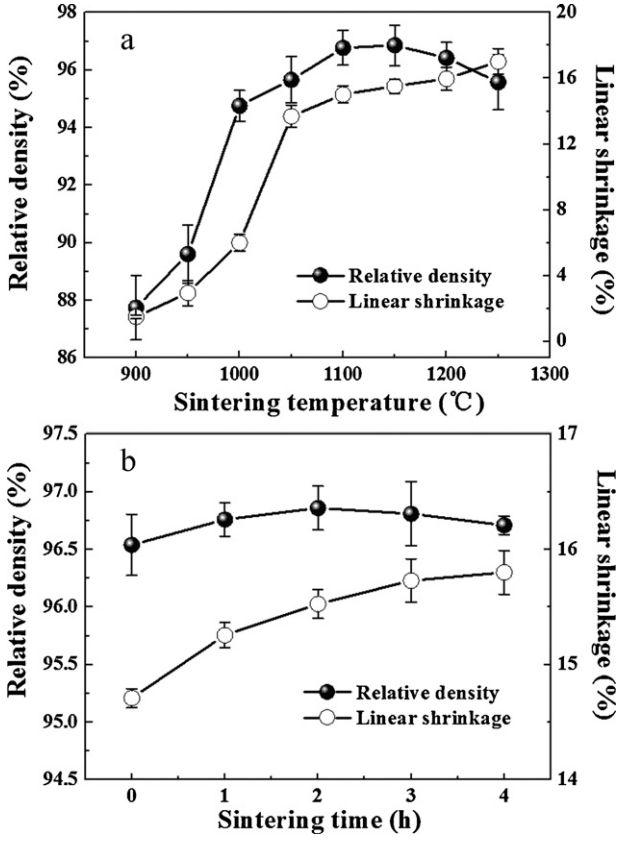

Fig. 2. Relative density and linear shrinkage of the PZT/ZnO_w composites sintered at different (a) sintering temperatures and (b) sintering times.

3. Results and discussion

Fig. 1(a) shows the SEM image of ZnO_w synthesized by the simple combustion oxidation method without any catalysts or additives. It is clearly seen that the nanostructures are definitely uniform. The individual structure consists of needle-shaped legs with high aspect ratio. The thickness of narrow tips is some decades of nanometer, whereas the lengths are in the range of 15–20 μm. The X-ray diffraction pattern of the as-synthesized products is shown in Fig. 1(b), where the diffraction peaks of ZnO are sharp and with narrow half width and the peaks of other impurity phase are not found. It indicates that the microstructure of the product is typical hexagonal and the strong intensities relative to the background signal further verify the high purity and high crystallinity of tetra-needle ZnO_w. Fig. 1(c) shows the SEM micrograph of polished surface for the sample sintered at 1150 °C for 2 h. The dark phases are ZnO_w, which are homogeneously dispersed in the

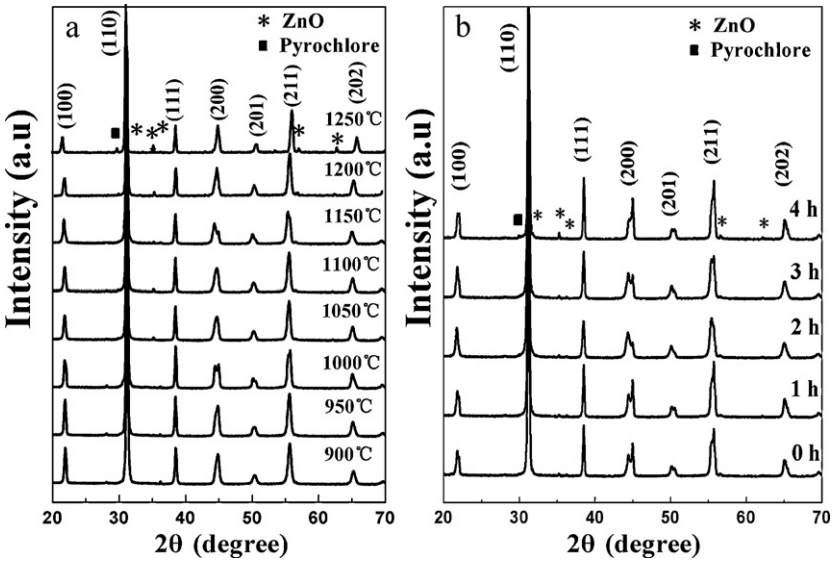

Fig. 3. XRD patterns of the PZT/ZnO_w composites sintered at different (a) sintering temperatures and (b) sintering times.

gray phases PZT [74,75]. The specifically enlarged morphology of ZnO_w embedded in the PZT matrix is shown in Fig. 1(d). It can be clearly observed that ZnO_w in the size of ~2 μm is located at the matrix grain boundaries and some debonding interfaces between whisker and matrix are present, which is also reported previously [75]. On the other hand, in our previous studies [74–77], we have observed ZnO diffraction peaks in the XRD patterns of the PZT/ZnO_w composites, even the content of ZnO_w is as low as 1 wt.%. It confirms that there is no serious chemical reaction occurring between PZT and ZnO_w in the composites and also no significant interface diffusion happens, though there could be some Zn^{2+} ions diffused into the PZT crystal structure and affected the electrical properties [76].

Fig. 2(a) shows the relative density ρ_r and linear shrinkage *d*% of the PZT/ZnO_w composites sintered for 2 h as a function of sintering temperature. Each value is the average of 3–5 samples, and the error bars represent the standard deviation. It can be seen that with the increase of sintering temperature from 900 to 1250 °C, the ρ_r of the composites increases sharply and then reaches the highest value of 96.86% at 1150 °C, after which ρ_r decreases slightly. On the other hand, the *d*% of the composites increases intensely before 1050 °C and then increases steadily. The ρ_r and *d*% of the PZT/ZnO_w composites sintered at 1150 °C as a function of sintering time is shown in Fig. 2(b). It is observed that all highly dense bodies of the PZT/ZnO_w composites are obtained at more than 96% of the theoretical density. Furthermore, with the increase of sintering

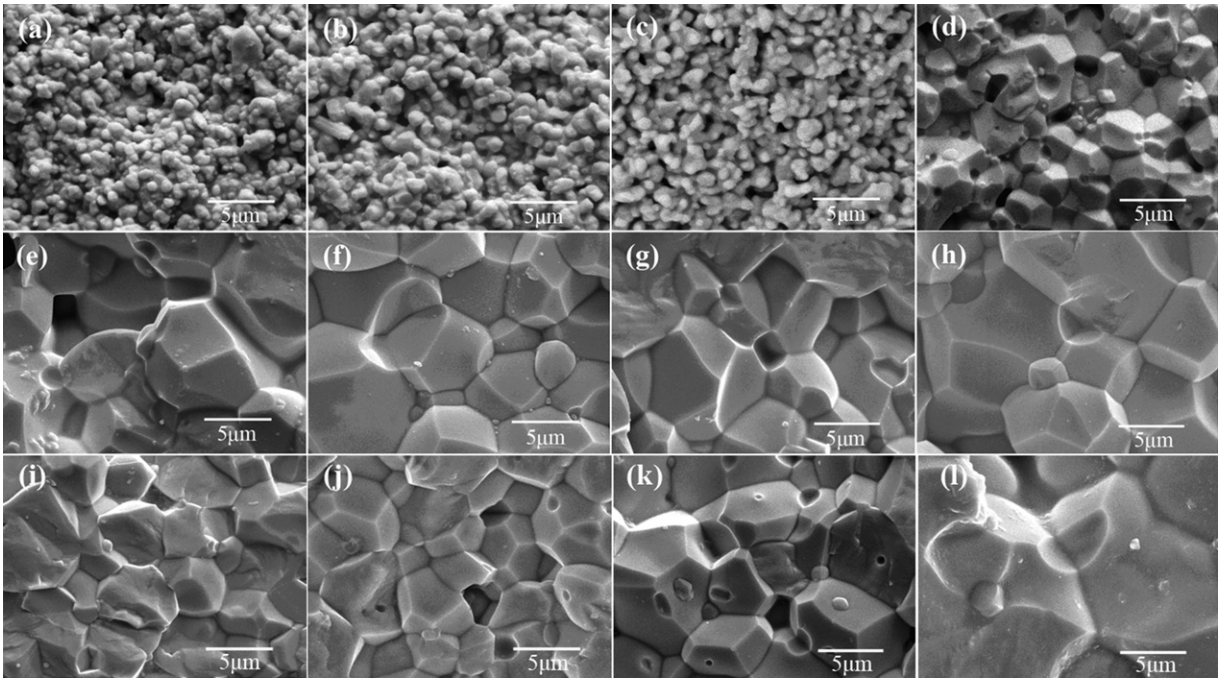

Fig. 4. SEM images of the PZT/ZnO_w composites sintered at different conditions: (a) 900 °C/2 h, (b) 950 °C/2 h, (c) 1000 °C/2 h, (d) 1050 °C/2 h, (e) 1100 °C/2 h, (f) 1150 °C/2 h, (g) 1200 °C/2 h, (h) 1250 °C/2 h, (i) 1150 °C/0 h, (j) 1150 °C/1 h, (k) 1150 °C/3 h and (l) 1150 °C/4 h.

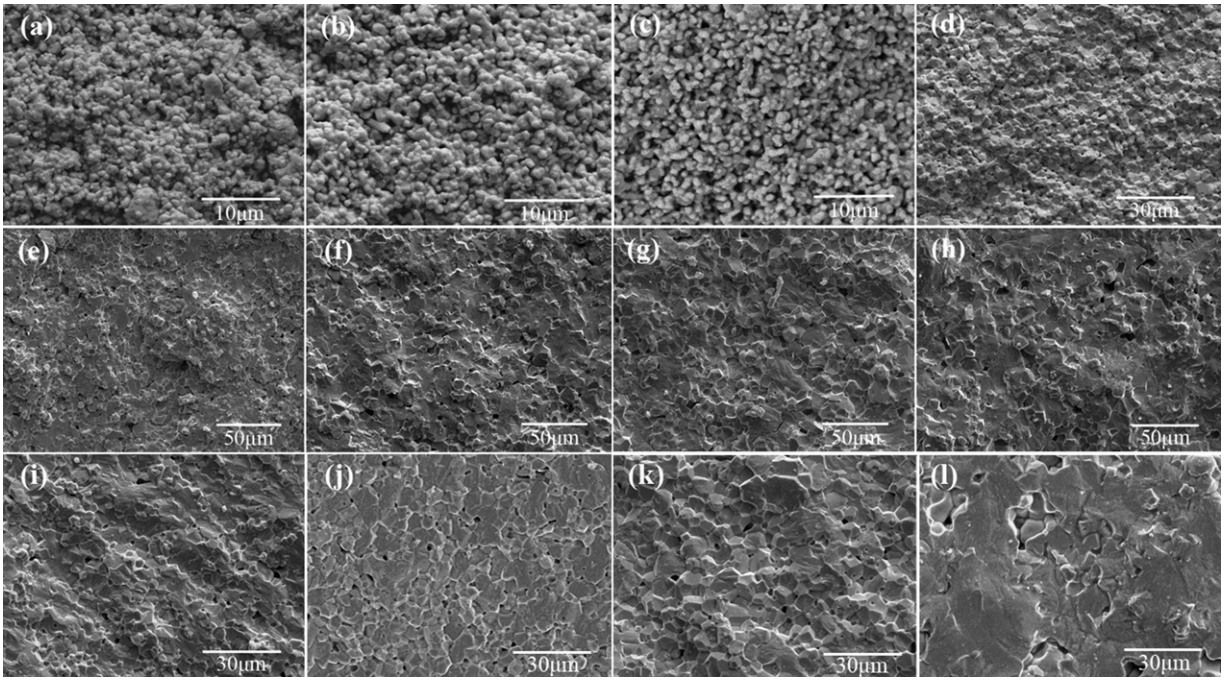

Fig. 5. SEM fractographs of fracture feature for the PZT/ZnO_w composites sintered at different conditions: (a) 900 °C/2 h, (b) 950 °C/2 h, (c) 1000 °C/2 h, (d) 1050 °C/2 h, (e) 1100 °C/2 h, (f) 1150 °C/2 h, (g) 1200 °C/2 h, (h) 1250 °C/2 h, (i) 1150 °C/0 h, (j) 1150 °C/1 h, (k) 1150 °C/3 h and (l) 1150 °C/4 h.

time, the ρ_r of the composites increases at first, reaching the highest value at 2 h and then decreases. However, the *d*% of the composites increases all the time. It is revealed that the densification of the PZT/ZnO_w composites is improved significantly with the increase of sintering temperature and time. However, the ρ_r of the composites decreases as the sintering temperature and time exceeds the optimum sintering condition (1150 °C for 2 h), which has negative effects on the microstructure and properties as discussed later.

Fig. 3(a) shows the XRD patterns of the PZT/ZnO_w composites sintered from 900 to 1250 °C for 2 h. The characteristic diffraction peaks of the PZT perovskite phase can be identified from all sintered composites. However, the diffraction peaks of ZnO in the composites are not intense, which is due to the small amount of ZnO_w. In addition, when the sintering temperature is over 1150 °C, the peaks of the pyrochlore phase are present, which is attributed to the high PbO evaporation rate of PZT system at high sintering temperature. Furthermore, the XRD patterns of the PZT/ZnO_w composites sintered at 1150 °C with different sintering times are shown in Fig. 3(b). All sintered composites present the PZT perovskite phase, and the diffraction peaks of ZnO in the composites are also not intense. However, with the sintering time increasing up to 4 h, the formation of the pyrochlore phase can be found in the XRD pattern, which is caused by the high PbO evaporation due to a long sintering time. As a consequence, excessive sintering temperature and time has negative effects on the phase structure of PZT and leads to the formation of pyrochlore phase.

Fig. 4(a)–(h) shows the SEM images of the PZT/ZnO_w composites sintered at different temperatures for 2 h. It is distinctly observed that as the sintering temperature increasing from 900 to 1250 °C, the grain size becomes larger, the cavities are reduced and the composites turn into dense structure gradually. In addition, the SEM images of the fracture surfaces of the PZT/ZnO_w composites sintered at 1150 °C from 0 to 4 h are shown in Fig. 4(i)–(l). We can see that all the sintered samples are dense and of granular structure. With the increase of sintering time, the grain size becomes larger.

According to the kinetic grain growth equation expressed as below [80,81]

$$\log G = \frac{1}{n}\log t + \frac{1}{n}\left(\log K_0 - 0.434\frac{Q}{RT}\right) \quad (1)$$

where G is the average grain size at the time, n is the kinetic grain growth exponent, t is the sintering time, K_0 is a constant, Q is the apparent activation energy, R is the gas constant, and T is the absolute temperature. It can be explained that the increase of sintering temperature and time could enhance the grain growth of the PZT/ZnO_w composites. However, as shown in Fig. 4(h) and (l), due to the high sintering temperature and long sintering time, the grain size of the composites partially becomes exceptionally huge, which may lead to the deterioration of the bulk density sintered over 1150 °C or 2 h [82].

Fig. 5(a)–(h) shows the SEM fractographs of the PZT/ZnO_w composites sintered from 900 to 1250 °C for 2 h. It is observed that with the increase of sintering temperature, the grain boundaries of the PZT/ZnO_w composites become more and more ambiguous, and the roughness of the fracture surface increases greatly. In other words, at low sintering temperatures, the fracture mode of the PZT/ZnO_w composites is completely intergranular. However, with the increase of sintering temperature, the fracture mode changes from intergranular to intragranular. Furthermore, the SEM fractographs of the PZT/ZnO_w composites sintered at 1150 °C from 0 to 4 h are shown in Fig. 5(i)–(l). It is seen that when the sintering time is 0 h (Fig. 5(i)), the fracture surface of the PZT/ZnO_w composites is rough and ambiguous, and the fracture mode is a mixture of transgranular and intergranular modes, where the degree of intergranular fracture decreases with the sintering time increasing. When the PZT/ZnO_w composites sintered for 4 h (Fig. 5(l)), the composites exhibit a flat fracture surface and the grain boundaries almost could not be found, resulting from its dominating transgranular fracture mode. It is revealed that the initiated cracks in the PZT/ZnO_w composites propagate mostly along intergranular and interphase boundaries when sintered at low temperatures (Fig. 5(a)–(d)). However, with the increase of sintering temperature and time, the cracks propagate more and more in the intragranular mode (Fig. 5(e)–(l)) and

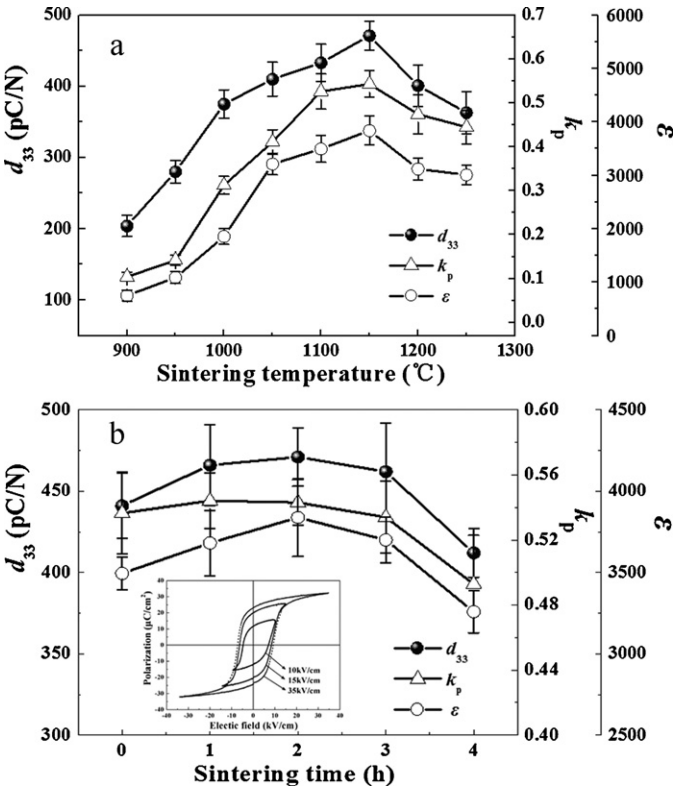

Fig. 6. Dependence of d_{33}, ε and k_p for the PZT/ZnO_w composites on the (a) sintering temperature and (b) sintering time. The inset in (b) is ferroelectric hysteresis loops of the PZT/ZnO_w composites sintered at 1150 °C for 2 h.

the fracture path is significantly extended into polyphase sinters, which indicates that the increase of sintering temperature and time reinforces grain boundaries of the PZT/ZnO_w composites [24].

Fig. 6(a) shows the d_{33}, k_p and ε of the PZT/ZnO_w composites sintered for 2 h as a function of the sintering temperature. The values of d_{33}, k_p and ε of the composites increase greatly with the sintering temperature up to 1150 °C and then decrease with further increasing the sintering temperature. In addition, the d_{33}, k_p and ε of the PZT/ZnO_w composites sintered at 1150 °C as a function of the sintering time is shown in Fig. 6(b). With the increase of sintering time, the values of d_{33}, k_p and ε increase at first and then decrease. The samples sintered at 1150 °C for 2 h possess the optimum d_{33}, k_p and ε values of 471 pC/N, 0.543 and 3838, respectively, where the highest ρ_r of 96.86% is also obtained as shown in Fig. 2. The promotion of d_{33}, k_p and ε below the optimum sintering condition is primarily attributed to the increased density, lowering leakage current and enhancing the poling process [83,84]. However, the decline of d_{33}, k_p and ε above the optimum sintering condition mainly due to the poor bulk density and the inclusion of the non-piezoelectric pyrochlore phase as discussed in Figs. 2 and 3 [85]. The ferroelectric hysteresis loops of PZT/ZnO_w sample sintered at 1150 °C for 2 h with different electric fields are shown in the inset of Fig. 6(b). It is observed that as the applied electric field increasing, the polarization increases and reaches to saturation at a substantially high applied field [86]. The remnant polarization P_r and coercive field E_c of the sample at 35 kV/cm electric field are 23.2 μC/cm^2 and 9.2 kV/cm, respectively.

In the light of the above discussion of densification, microstructure and piezoelectric properties, the investigation of the PZT/ZnO_w composites should be focused on the sintering temperature of 1150 °C and sintering time of 2 h. The dependence of d_{33} and ε of the PZT/ZnO_w composites on various poling conditions is investigated as shown in Fig. 7. With the increase of poling temperature,

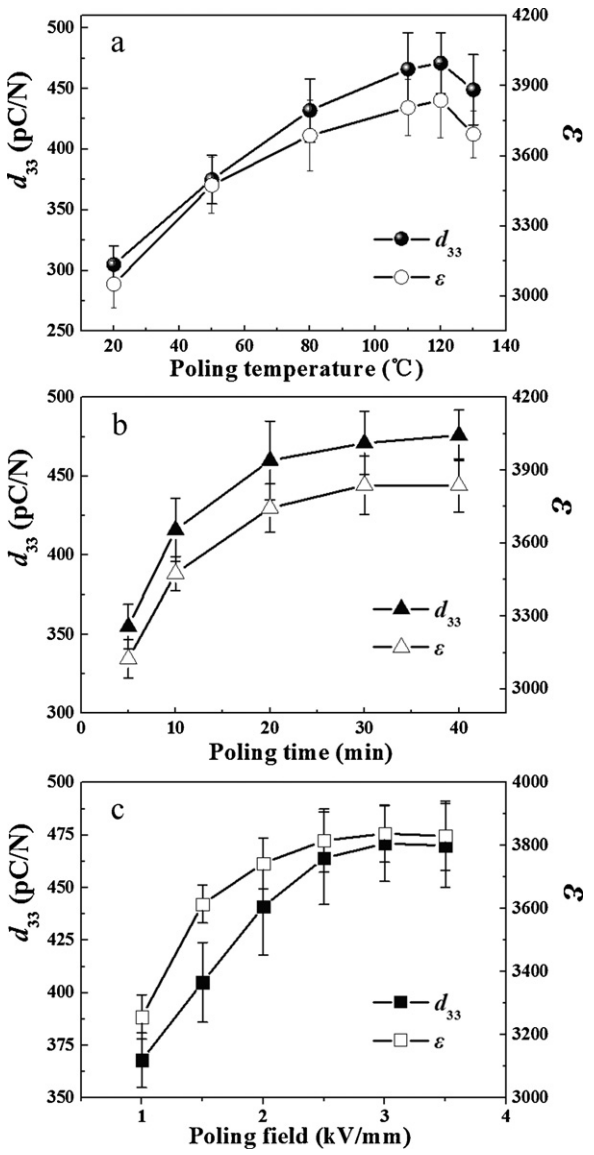

Fig. 7. Dependence of d_{33} and ε on the (a) poling temperature, (b) poling time and (c) poling field for the PZT/ZnO_w composites sintered at 1150 °C for 2 h.

the values of d_{33} and ε of the composites increase greatly with the poling temperature up to 120 °C and then decrease (Fig. 7(a)). The values of d_{33} and ε of the composites at the poling temperature of 120 °C become saturated as the poling time and field are higher than 30 min (Fig. 7(b)) and 3 kV/mm (Fig. 7(c)), respectively.

For further practical application, the temperature and time stability of the PZT/ZnO_w composites has been investigated as shown in Fig. 8. Fig. 8(a) shows the temperature dependence of ε and k_p for the composites sintered at 1150 °C for 2 h. In the temperature range of 0–100 °C, the values of ε increase linearly with the increase of temperature, while k_p changes slightly with the variation of below 10%. The improvement of ε with the increase of sintering temperature is ascribed to the enhancement of permittivity, which is induced by the aggravated thermal motion and the triggered increase of thermal defects in the composites. The aging problems of ε and k_p obtained for the PZT/ZnO_w composites sintered at 1150 °C for 2 h are observed from the very initial time of preparation at room temperature as shown in Fig. 8(b). After 60 days, the values of ε and k_p slightly decrease by 2% and 3%, respectively, which may be linked to the relaxation of domain walls or humidity sensitivity of PZT [87]. The results show that the

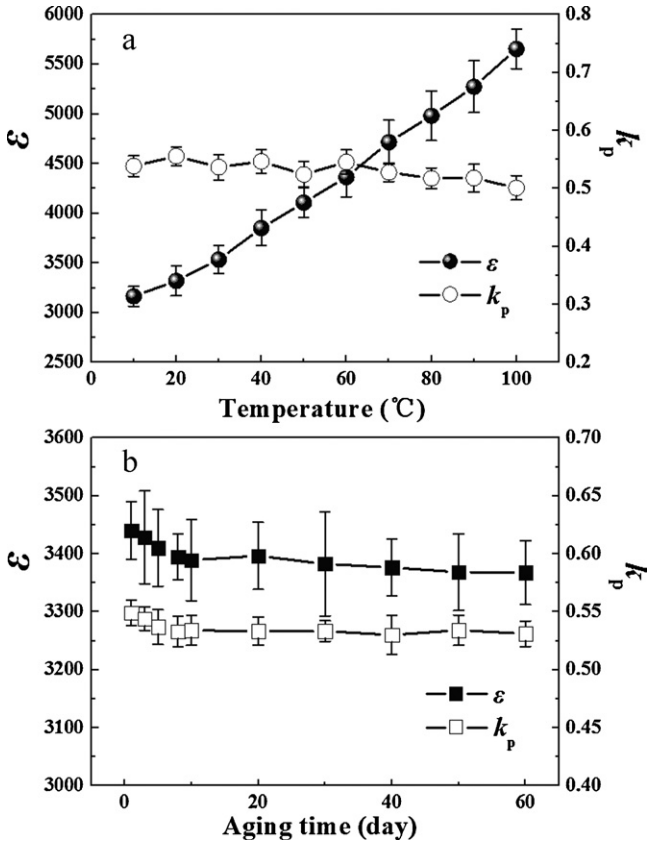

Fig. 8. (a) Temperature dependence and (b) aging behavior of ε and k_p for the PZT/ZnO_w composites sintered at 1150 °C for 2 h.

PZT/ZnO_w composites possess good temperature and time stability, which is vital for practical applications.

4. Conclusions

In summary, the sintering, microstructure and electrical properties of the PZT piezoelectric composites incorporated with ZnO_w have been investigated in different sintering conditions of sintering temperature from 900 to 1250 °C and sintering time from 0 to 4 h. The increase of sintering temperature and time enhanced the grain growth, densification and electrical properties in effect. However, as the sintering temperature exceeded 1150 °C, the density and electrical properties deteriorated seriously. The PZT/ZnO_w composites with 2 wt.% ZnO_w sintered at 1150 °C for 2 h showed the optimal density of $\rho_r \sim 96.86\%$ and electrical properties of $d_{33} \sim 471$ pC/N, $\varepsilon \sim 3838$, $k_p \sim 0.543$, $P_r \sim 23.2\ \mu C/cm^2$ and $E_c \sim 9.2$ kV/cm. Furthermore, the temperature and time stability of the PZT/ZnO_w composites was quite good, suggesting that the new PZT/ZnO_w composites were promising candidates for practical applications.

Acknowledgements

This research was supported by the National Natural Science Foundation of China under Grant Nos. 50742007, 50872159 and 50972014, the National High Technology Research and Development Program of China under Grant No. 2007AA03Z103, the National Defense Fund under Grant No. 401050301 and the Key Laboratory Foundation of Sonar Technology of China under Grant No. 9140C24KF0901.

References

[1] G.H. Haertling, J. Am. Ceram. Soc. 82 (1999) 797–818.
[2] Z.P. Yang, Y.T. Hou, H. Pan, Y.F. Chang, J. Alloys Compd. 480 (2009) 246–253.
[3] Y. Cheng, Y. Yang, Y.P. Wang, H.Q. Meng, J. Alloys Compd. 508 (2010) 364–369.
[4] M.A. Mohiddon, K.L. Yadav, Phys. Status Solidi A 206 (2009) 1606–1615.
[5] C.Q. Liu, W.L. Li, W.D. Fei, S.Q. Zhang, J.N. Wang, J. Alloys Compd. 493 (2010) 499–501.
[6] S.J. Zhang, R. Xia, L. Lebrun, D. Anderson, T.R. Shrout, Mater. Lett. 59 (2005) 3471–3475.
[7] S. Pruvost, L. Lebrun, G. Sebald, L. Seveyrat, D. Guyomar, S.J. Zhang, T.R. Shrout, J. Appl. Phys. 100 (2006) 074104.
[8] R.E. Eitel, S.J. Zhang, T.R. Shrout, C.A. Randall, I. Levin, J. Appl. Phys. 96 (2004) 2828–2831.
[9] S.J. Zhang, C.A. Randall, T.R. Shrout, Appl. Phys. Lett. 83 (2003) 3150–3152.
[10] Z.H. Yao, H.X. Liu, M.H. Cao, H. Hao, J. Alloys Compd. 505 (2010) 281–285.
[11] K. Ramam, A.J. Bell, C.R. Bowen, K. Chandramouli, J. Alloys Compd. 473 (2009) 330–335.
[12] X.L. Chao, Z.P. Yang, Y.F. Chang, M.Y. Dong, J. Alloys Compd. 477 (2009) 243–249.
[13] X.L. Chao, D.F. Ma, R. Gu, Z.P. Yang, J. Alloys Compd. 491 (2010) 698–702.
[14] A.S. Fawzi, A.D. Sheikh, V.L. Mathe, J. Alloys Compd. 493 (2010) 601–608.
[15] D.W. Wang, D.Q. Zhang, J. Yuan, Q.L. Zhao, H.M. Liu, Z.Y. Wang, M.S. Cao, Chin. Phys. B 18 (2009) 2596–2602.
[16] X.L. Chao, Z.P. Yang, L.R. Xiong, Z. Li, J. Alloys Compd. 509 (2011) 512–517.
[17] F. Gao, R.Z. Hong, J.J. Liu, Z. Li, L.H. Cheng, C.S. Tian, J. Alloys Compd. 475 (2009) 619–623.
[18] R.V. Paia, R. Mishra, M.R. Pai, S.K. Mukerjee, V. Venugopal, J. Alloys Compd. 508 (2010) 184–190.
[19] S. Roy, B.S.S. Chandra Rao, J. Subrahmanyam, Scripta Mater. 57 (2007) 1024–1027.
[20] R. Fu, T.Y. Zhang, J. Am. Ceram. Soc. 83 (2000) 1215–1218.
[21] D.W. Wang, M.S. Cao, J. Yuan, Q.L. Zhao, H.B. Li, D.Q. Zhang, S. Agathopoulos, J. Am. Ceram. Soc. 94 (2011) 647–650.
[22] Z.G. Zhou, B. Wang, Y.G. Sun, Int. J. Solids Struct. 40 (2003) 747–762.
[23] Z.G. Zhou, B. Wang, Appl. Math. Mech. -Engl. 28 (2007) 417–428.
[24] K. Tajima, H.J. Hwang, M. Sandob, K. Niihara, J. Eur. Ceram. Soc. 19 (1999) 1179–1182.
[25] H.B. Lin, M.S. Cao, J. Yuan, D.W. Wang, Q.L. Zhao, F.C. Wang, Chin. Phys. B 17 (2008) 4323–4327.
[26] Y. Bao, P.S. Nicholson, J. Am. Ceram. Soc. 90 (2007) 1063–1070.
[27] G.C. Quan, K.T. Conlon, D.S. Wilkinson, J. Eur. Ceram. Soc. 27 (2007) 389–396.
[28] D.Q. Zhang, D.W. Wang, J. Yuan, Q.L. Zhao, Z.Y. Wang, M.S. Cao, Chin. Phys. Lett. 25 (2008) 4410–4413.
[29] Y.G. Wu, T.C. Feng, J. Alloys Compd. 491 (2010) 452–455.
[30] C. Puchmark, S. Jiansirisomboon, G. Rujijanagul, T.P. Comyn, J.Y. He, S.J. Milne, Mater. Res. Bull. 42 (2007) 1269–1277.
[31] M.S. Cao, D.W. Wang, J. Yuan, H.B. Lin, Q.L. Zhao, D.Q. Zhang, Mater. Lett. 64 (2010) 1798–1801.
[32] S. Jiansirisomboon, T. Sreesattabud, A. Watcharapasorn, Ceram. Inter. 34 (2008) 719–722.
[33] S. Jiansirisomboon, M. Promsawat, O. Namsar, A. Watcharapasorn, Mater. Chem. Phys. 117 (2009) 80–85.
[34] O. Namsar, A. Watcharapasorn, S. Jiansirisomboon, Phys. Scr. T139 (2010) 014001.
[35] D.W. Wang, H.B. Jin, J. Yuan, B.L. Wen, Q.L. Zhao, D.Q. Zhang, M.S. Cao, Chin. Phys. Lett. 27 (2010) 047701.
[36] H.L. Zhang, J.F. Li, B.P. Zhang, J. Am. Ceram. Soc. 89 (2006) 1300–1307.
[37] H.L. Zhang, J.F. Li, B.P. Zhang, W. Jiang, Mater. Sci. Eng. A 498 (2008) 272–277.
[38] H.L. Zhang, S. Yang, B.P. Zhang, J.F. Li, Mater. Chem. Phys. 122 (2010) 237–240.
[39] Z.L. Wang, J.H. Song, Science 312 (2006) 242–246.
[40] Y.N. Zhao, M.S. Cao, H.B. Jin, L. Zhang, C.J. Qiu, Scripta Mater. 54 (2006) 2057–2061.
[41] Y.X. Du, F.G. Zeng, J. Alloys Compd. 509 (2011) 1275–1278.
[42] T. Al-Harbi, J. Alloys Compd. 509 (2011) 387–390.
[43] R. Yousefi, B. Kamaluddin, J. Alloys Compd. 479 (2009) L11–L14.
[44] Q. Wan, J. Huang, A.X. Lu, T.H. Wang, Appl. Phys. Lett. 93 (2008) 103109.
[45] V. Goyal, K.P. Bhatti, S. Chaudhary, J. Alloys Compd. 508 (2010) 419–425.
[46] G.N.S. Vijayakumar, S. Devashankar, M. Rathnakumari, P. Sureshkumar, J. Alloys Compd. 507 (2010) 225–229.
[47] M.L. Dinesha, H.S. Jayanna, S. Mohanty, S. Ravi, J. Alloys Compd. 490 (2010) 618–623.
[48] Z.W. Zhou, L.S. Chu, S.C. Hu, Mater. Sci. Eng. B 126 (2006) 93–96.
[49] M.S. Cao, X.L. Shi, X.Y. Fang, H.B. Jin, Z.L. Hou, W. Zhou, Appl. Phys. Lett. 91 (2007) 203110.
[50] B.K. Sharma, N. Khare, S.K. Dhawan, H.C. Guptaa, J. Alloys Compd. 477 (2009) 370–373.
[51] C.H. Hsu, J. Alloys Compd. 464 (2008) 412–417.
[52] S.Q. Yu, B. Tang, S.R. Zhang, X.H. Zhou, J. Alloys Compd. 505 (2010) 814–817.
[53] X.Y. Fang, M.S. Cao, X.L. Shi, Z.L. Hou, W.L. Song, J. Yuan, J. Appl. Phys. 107 (2010) 054304.
[54] X.Y. Fang, X.L. Shi, M.S. Cao, J. Yuan, J. Appl. Phys. 104 (2008) 096101.
[55] X.L. Chen, Z.W. Zhou, W.C. Lv, T. Huang, S.C. Hu, Mater. Chem. Phys. 115 (2009) 258–262.
[56] G. Liu, G.S. Li, X.Q. Qiu, L.P. Li, J. Alloys Compd 481 (2009) 492–497.
[57] Q.L. Zhao, M.S. Cao, J. Yuan, W.L. Song, R. Lu, D.W. Wang, D.Q. Zhang, J. Alloys Compd. 492 (2010) 264–268.

[58] S.J. Li, L. Ge, H.T. Gu, Y.F. Zheng, H. Chen, L.C. Guo, J. Alloys Compd. 509 (2011) 94–98.
[59] C.H. Hsu, C.Y. Chung, J. Alloys Compd. 491 (2010) 483–486.
[60] Q.L. Zhao, M.S. Cao, J. Yuan, R. Lu, D.W. Wang, D.Q. Zhang, Mater. Lett. 64 (2010) 632–635.
[61] C.H. Hsu, Y.S. Chang, J. Alloys Compd. 479 (2009) 714–718.
[62] C.L. Huang, Y.B. Chen, M.L. Lee, J. Alloys Compd. 469 (2009) 357–361.
[63] Y.B. Chen, J. Alloys Compd. 478 (2009) 781–784.
[64] A. Banerjee, A. Bandyopadhyay, S. Bose, J. Am. Ceram. Soc. 89 (2006) 1594–1600.
[65] X. Zeng, A.L. Ding, T. Liu, G.C. Deng, X.S. Zheng, W.X. Cheng, J. Am. Ceram. Soc. 89 (2006) 728–730.
[66] C.W. Ahn, H.C. Song, S. Nahm, S. Priya, S.H. Park, K. Uchino, H.G. Lee, H.J. Lee, J. Am. Ceram. Soc. 89 (2006) 921–925.
[67] H. Li, Z.P. Yang, L.L. Wei, Y.F. Chang, Mater. Res. Bull. 44 (2009) 638–643.
[68] X.L. Chao, Z.P. Yang, X.H. Huang, D.F. Ma, J.H. Zeng, Curr. Appl. Phys. 9 (2009) 1283–1287.
[69] M.S. Cao, W. Zhou, X.L. Shi, Y.J. Chen, Appl. Phys. Lett. 91 (2007) 021912.
[70] Z.X. Guo, J. Xiong, M. Yang, W. Li, J. Alloys Compd. 461 (2008) 342–345.
[71] J.L. Rong, X. Wang, M.S. Cao, D.W. Wang, W. Zhou, T.F. Xu, Chin. Phys. Lett. 27 (2010) 066201.
[72] M.S. Cao, W.L. Song, W. Zhou, D.W. Wang, J.L. Rong, J. Yuan, S. Agathopoulos, Compos. Struct. 92 (2010) 2984–2991.
[73] J. Shi, Y. Wang, L. Liu, H.W. Bai, J. Wu, C.X. Jiang, Z.W. Zhou, Mater. Sci. Eng. A 512 (2009) 109–116.
[74] H.B. Lin, M.S. Cao, Q.L. Zhao, X.L. Shi, D.W. Wang, F.C. Wang, Scripta Mater. 59 (2008) 780–783.
[75] J. Yuan, D.W. Wang, H.B. Lin, Q.L. Zhao, D.Q. Zhang, M.S. Cao, J. Alloys Compd. 504 (2010) 123–128.
[76] D.W. Wang, M.S. Cao, J. Yuan, H.B. Lin, Q.L. Zhao, D.Q. Zhang, Curr. Nanosci. 7 (2011) 227–234.
[77] D.W. Wang, M.S. Cao, J. Yuan, Q.L. Zhao, H.B. Li, H.B. Lin, D.Q. Zhang, J. Mater. Sci. Mater. Electron (2011), doi:10.1007/s10854-011-0319-8.
[78] Y.N. Zhao, M.S. Cao, H.B. Jin, X.L. Shi, X. Li, S. Agathopoulos, J. Nanosci. Nanotechnol. 6 (2006) 2525–2528.
[79] X.L. Shi, M.S. Cao, Y.N. Zhao, W.L. Song, J.L. Rong, Sci. China Ser. E-Tech. Sci. 51 (2008) 1433–1438.
[80] T. Senda, R.C. Bradt, J. Am. Ceram. Soc. 73 (1990) 106–114.
[81] T.Y. Chen, S.Y. Chu, Y.D. Juang, Sens. Actuator A Phys. 102 (2002) 6–10.
[82] R.C. Chang, S.Y. Chu, Y.P. Wong, C.S. Hong, H.H. Huang, J. Alloys Compd. 456 (2008) 308–312.
[83] S.H. Park, C.W. Ahn, S. Nahm, J.S. Song, Jpn. J. Appl. Phys. 43 (2004) L1072–L1074.
[84] M. Kosec, V. Bobnar, M. Hrovat, J. Bernard, B. Malic, J. Holc, J. Mater. Res. 19 (2004) 1849–1854.
[85] J.J. Choi, B.D. Hahn, D.S. Park, W.H. Yoon, J.H. Lee, J. Am. Ceram. Soc. 90 (2007) 388–392.
[86] N. Vittayakorn, G. Rujijanagul, D.P. Cann, Curr. Appl. Phys. 7 (2007) 582–585.
[87] H. Birol, D. Damjanovic, N. Setter, J. Eur. Ceram. Soc. 26 (2006) 861–866.